DISK methods for yield fluids

Karol Cascavita

Directed by: Alexandre Ern
Supervised by: Xavier Château, Jeremy Bleyer

University Paris-Est, CERMICS, NAVIER (ENPC)

CERMICS Young Researchers Seminar

Outline

1 Yield Fluids

Outline

1. Yield Fluids
2. Discontinuous Skeletal Methods

Outline

1. Yield Fluids
2. Discontinuous Skeletal Methods
3. Results

Outline

1. Yield Fluids
2. Discontinuous Skeletal Methods
3. Results
4. Conclusions

Yield Fluids: Motivation

Growing interest due to a wide range of applications:

- Flow of viscoplastic(yield) fluids : civil engineering, materials processing, petroleum drilling operations, food and cosmetics industry.
- Bubbles in viscoplastic flows: Aerated building materials, mousse.

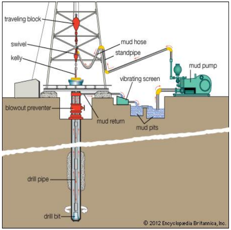

Figure: Examples of applications

Yield Fluids: Challenges

- Viscoplastic materials are non-Newtonian fluids that require a finite yield stress to flow (solid or fluid-like behavior)
- Yield stress fluids are governed by a non-regular and non-linear constitutive equation
- Solid/liquid boundary not known a *priori*
- Viscoplastic materials constitute a challenging problem theoretically and experimentally
- Scarce analysis, experimental and numerical data in the literature
- Classical FEM simulations methods are costly for iterative solvers: Not naturally fitted for parallelization.
- Discontinuous skeletal methods are a promising tool to replace FEM.

Yield Fluids: Model problem I

- Let $\Omega \subset R^d$, $d \geqslant 1$, denote a d-dimensional open bounded and connected domain
- For a source term $\mathbf{f} \in L^2(\Omega)^d$
- Momentum and mass conservation for incompressible flows:

$$
\begin{aligned}
\operatorname{div} \boldsymbol{\sigma}_{\mathbf{t}} + \mathbf{f} &= \mathbf{0} && \text{in} \quad \Omega, \\
\operatorname{div} \mathbf{u} &= 0 && \text{in} \quad \Omega, \\
\mathbf{u} &= \mathbf{0} && \text{on} \quad \partial\Omega,
\end{aligned}
$$

  with $\sigma_{\mathbf{t}}$ total stress tensor and $\mathbf{u}$ the unknown velocity field.

- Spheric and deviatoric parts:

$$
\boldsymbol{\sigma}_t = \boldsymbol{\sigma}_D - \frac{1}{3} tr(\boldsymbol{\sigma}_t)\mathbf{I} \tag{1}
$$

Yield Fluids: Model problem II

Viscoplastic fluid model: Bingham model

$$\begin{cases} \boldsymbol{\sigma}_D = 2\mu\nabla_s\mathbf{u} + \sqrt{2}\tau_0\dfrac{\nabla_s\mathbf{u}}{|\nabla_s\mathbf{u}|} & \text{when } \sqrt{\frac{1}{2}}|\boldsymbol{\sigma}_D| > \tau_0 \\ \nabla_s\mathbf{u} = 0 & \text{otherwise} \end{cases}$$

- with $\tau_0 \geqslant 0$ and $\mu > 0$ denoting the viscosity and the yield stress respectively.
- $\nabla_s\mathbf{u}$ the symmetric gradient.
- We use the Frobenius norm $|\boldsymbol{\tau}| = \sqrt{\boldsymbol{\tau} : \boldsymbol{\tau}}$

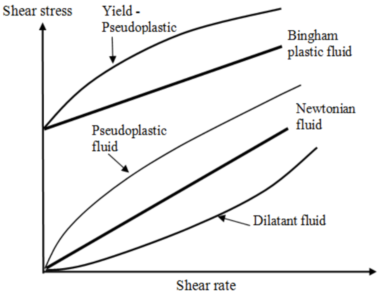

Figure: Clasification of fluids

Yield Fluids: Model problem II

- Glowinski [2] showed the PDEs can be recast as a minimization problem:

$$\mathbf{u} = \arg\min_{\mathbf{v}\in K(\mathbf{0})} \int_\Omega \mathcal{D}(\mathbf{v})d\Omega - \int_\Omega \mathbf{f}\cdot\mathbf{v}$$

where $K(\mathbf{u}_D)$ is the kernel of the divergence operator and defined as $K(\mathbf{u}_D) = \left\{\mathbf{v} \in L_2(\Omega)^d | \text{div } \mathbf{v} = 0 \in \Omega, \mathbf{u} = \mathbf{u}_D \in \partial\Omega\right\}$,

- The dissipation energy

$$\mathcal{D}(\mathbf{u}) = \mu|\nabla_s \mathbf{u}|^2 + \sqrt{2}\tau_0|\nabla_s \mathbf{u}|,$$

Yield Fluids: Augmented Lagrangian Algorithm

- Solve the saddle problem

$$(\mathbf{u}, \gamma, \sigma) = \min_{\mathbf{v} \in \mathbf{H}_0^1, \delta \in \mathfrak{L}_2} \max_{\tau \in \mathfrak{L}_2} \mathcal{L}(\mathbf{v}, \delta, \boldsymbol{\tau})$$

- New constraint $\boldsymbol{\gamma} = \nabla_s \mathbf{u}$
- Augmented Lagrangian:

$$\begin{aligned} \mathcal{L}(\mathbf{u}, \gamma, \boldsymbol{\sigma}) &= \frac{\mu}{2} \int_\Omega |\gamma|^2 d\Omega + \tau_0 \int_\Omega |\gamma| d\Omega - \int_\Omega \mathbf{f} \cdot \mathbf{u} d\Omega \\ &\quad + \int_\Omega \boldsymbol{\sigma} : (\nabla_s \mathbf{u} - \gamma) d\Omega + \frac{\alpha}{2} \int_\Omega |\nabla_s \mathbf{u} - \gamma|^2 d\Omega \end{aligned}$$

with $\alpha > 0$ is the augmentation parameter.

ALG: Uzawa-like algorithm, n^{th}-iteration

- Weak formulation: Assume $\boldsymbol{\sigma}^n$ and γ^n, then find $\mathbf{u}^n \in V, \forall \mathbf{v} \in \mathbf{H}_0^1(\Omega)^d$ such that

$$2\alpha(\nabla_s \mathbf{u}^{n+1}, \nabla_s \mathbf{v}) = (\mathbf{f}, \mathbf{v}) - (\boldsymbol{\sigma}^n - 2\alpha\gamma^n, \nabla_s \mathbf{v}),$$

- Solve point-wise

$$\gamma^{n+1}(\mathbf{x}) = \max\left(0, \frac{1}{(2\alpha+\mu)} \frac{\mathbf{X}^{n+1}(\mathbf{x})}{|\mathbf{X}^{n+1}(\mathbf{x})|}\left(|\mathbf{X}^{n+1}(\mathbf{x})| - \tau_0\right)\right)$$

where $\mathbf{X}^{n+1} = \boldsymbol{\sigma}^n + \alpha\nabla_s \mathbf{u}^{n+1}$.

- Update the stress

$$\boldsymbol{\sigma}^{n+1} = \boldsymbol{\sigma}^n + \alpha(\nabla_s \mathbf{u}^{n+1} - \gamma^{n+1}).$$

Discontinuous Skeletal methods

- There are differente kinds of DiSk methods: MFD, HFV, HDG, **HHO**. **Di**scontinuous **Sk**eletal methods approximate solutions of BVPs by
  - using discontinuous polynomials in the mesh skeleton
  - attaching unknowns to mesh faces
- Salient features:
  - Dimension-independent construction
  - Supportgeneral meshes(conforming and non-conforming)
  - Arbitrary polynomial order

DISK methods

In this work we use the Hybrid High Order method, introduced recently by Di Pietro et Ern [1, 3] for linear elasticity.
Attractive features:

- Designed from primal formulation
- Arbitrary order of polynomials.
- Suitable for hp-adaptivity.
- They can be applied to a fair range of PDE's.
- Gradient reconstruction based on local Neumann problems.

Degrees of freedom I

- We consider as model problem the laplace equation: $-\Delta u = f \ \in \Omega$
- Cell-Face based method: Hybrid method.
- DoFs are polynomials of order $k \geqslant 0$ attached to the mesh cells and their faces.

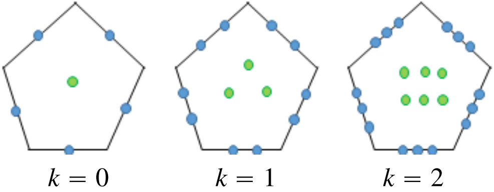

Figure: DOFs for k =0, 1, 2.

- We define for all $T \in \mathcal{T}_h$ the local space

$$\underline{\mathbf{U}}_h^k = \mathbb{P}_d^k(T) \times \left\{ \bigtimes_{F \in \mathcal{F}_h} \mathbb{P}_{d-1}^k(F) \right\}$$

Gradient reconstruction I

- The local potential reconstruction operator: $r_T^{k+1} : \underline{U}_T^k \to \mathbb{P}_d^{k+1}(T)$
- The local gradient reconstruction operator: $\nabla r_T^{k+1} : \underline{U}_T^k \to \nabla\mathbb{P}_d^{k+1}(T)$
- Let $\underline{v} \in \underline{U}_T^k$, then $\nabla r_T^{k+1}\underline{v} = \nabla s$ with $s \in \mathbb{P}_d^{k+1}(T)$
- ∇s solves the local problem for all $w \in \mathbb{P}_d^{k+1}(T)$

$$(\nabla s, \nabla w)_T = (\nabla v_T, \nabla w)_T + \sum_{F\in\mathcal{F}_T} (v_F - v_T, \nabla w \cdot \mathbf{n}_{TF})_F$$

- Reconstruction operator derives from integration by parts formula.
- Set $\int_T r_T^{k+1}\underline{v} = \int_T v_T$ then the reconstructed function is in $\mathbb{P}_d^k(T)$ and is unique.

Gradient reconstruction II

- Local interpolation operator $I_T^k : H^1(T) \to \underline{U}_T^k$, that maps a given function $v \in H^1(T)$ into the broken space of local collection of velocities.

$$I_T^k v = (\pi_T^k v, (\pi_F^k v)_{F \in \mathcal{F}_T}),$$

- Conmuting diagram property

$$\begin{tikzcd} H^1(T) \arrow[r, "\nabla"] \arrow[d, "\mathrm{I}_T^k"] & L^2(T)^d \arrow[d, "\pi_{\nabla \mathbb{P}_d^{k+1}(T)}"] \\ \mathrm{U}_T^k \arrow[r, "\underline{G}_T^k"] & \nabla \mathbb{P}_d^{k+1}(T) \end{tikzcd}$$

For all $u \in H^1(T)$ and all $w \in \mathbb{P}_d^{k+1}(T)$

$$(\nabla r_T^{k+1} I_T^k v, \nabla w)_T = (\nabla u, \nabla w)_T \qquad (2)$$

- Thus, $r_T^{k+1} I_T^k$ is the elliptic operator on $\mathbb{P}_d^{k+1}(T)$

Reconstruction operator III

Reconstruction operator $r_T^{k+1}\underline{\mathrm{v}}$ is used to build the following bilinear form on $U_T^k \times U_T^k$:

$$a_T^{(1)}(\underline{\mathrm{v}}, \underline{\mathrm{w}}) = (\nabla r_T^{k+1}\underline{\mathrm{v}}, \nabla r_T^{k+1}\underline{\mathrm{w}})_T$$

Note how $(\nabla r_T^{k+1}\underline{\mathrm{v}}, \nabla r_T^{k+1}\underline{\mathrm{w}})_T$ mimics *locally* the l.h.s. of our original problem

$$\text{Find } u \in H_0^1(\Omega) \text{ s.t. } (\nabla u, \nabla v)_\Omega = (f, v)_\Omega, \quad \forall v \in H_0^1(\Omega)$$

Stabilization operator I

- For $\underline{v} \in \underline{U}_T^k$, the reconstructed gradient $\nabla r_T^{k+1}\underline{v}$ is not stable: $\nabla r_T^{k+1}\underline{v} = 0$ *does not imply* that v_T and $v_{\partial T}$ are constant functions taking the same value.
- We introduce a least-squares penalization of the difference between functions in the faces and function in the cell

$$S_T^k\underline{v} := \pi_{\partial T}^k \left(v_{\partial T} - (v_T + r_T^{k+1}\underline{v} - \pi_T^k r_T^{k+1}\underline{v})|_{\partial T} \right),$$

Stabilization operator II

Using the stabilization operator just defined, we build a second bilinear form on $U_T^k \times U_T^k$:

$$s_T(\underline{v}, \underline{w}) = \sum_{F \in \mathcal{F}_{\partial T}} h_F^{-1} (S_T^k \underline{v}, S_T^k \underline{w})_F,$$

where h_F denotes the diameter of the face F.

- The stabilization as defined allows HHO to converge as $k+2$ in L_2 norm
- The simpler stabilization considering the difference $v_{\partial T} - v_T$ would limit convergence to $k+1$

Global spaces

Local discrete spaces U_T^k, for all $T \in \mathcal{T}$, are collected into a global discrete space

$$\underline{U}_h^k := U_{\mathcal{T}}^k \times U_{\mathcal{F}}^k,$$

where

$$U_{\mathcal{T}}^k := \mathbb{P}_d^k(\mathcal{T}) := \{v_{\mathcal{T}} = (v_T)_{T\in\mathcal{T}} \mid v_T \in \mathbb{P}_d^k(T),\ \forall T \in \mathcal{T}\},$$
$$U_{\mathcal{F}}^k := \mathbb{P}_{d-1}^k(\mathcal{F}) := \{v_{\mathcal{F}} = (v_F)_{F\in\mathcal{F}} \mid v_F \in \mathbb{P}_{d-1}^k(F),\ \forall F \in \mathcal{F}\}.$$

For a pair $\underline{v}_h := (v_{\mathcal{T}}, v_{\mathcal{F}})$ in the global discrete space $\underline{u}_h^k$, we denote $\underline{v}$, for all $T \in \mathcal{T}$, its restriction to the local discrete space U_T^k, where $v_{\partial T} = (v_F)_{F\in\mathcal{F}_{\partial T}}$
Homogeneous Dirichlet BCs are enforced strongly by considering the subspace

$$U_{h,0}^k := U_{\mathcal{T}}^k \times U_{\mathcal{F},0}^k,$$

where

$$U_{\mathcal{F},0}^k := \{v_{\mathcal{F}} \in U_{\mathcal{F}}^k \mid v_F \equiv 0,\ \forall F \in \mathcal{F}^{\mathrm{b}}\}.$$

Discrete problem

For all $T \in \mathcal{T}$, we combine reconstruction and stabilization bilinear forms into a_T on $\underline{U}_T^k \times \underline{U}_T^k$ such that

$$a_T := a_T^{(1)} + s_T.$$

We then do a standard cell-wise assembly

$$a_h(\underline{u}_h, \underline{w}_h) := \sum_{T \in \mathcal{T}} a_T(\underline{u}, \underline{w}),$$
$$\ell_h(\underline{w}_h) := \sum_{T \in \mathcal{T}} (f, w_T)_T.$$

Finally we search for $\underline{u}_h := (u_{\mathcal{T}}, u_{\mathcal{F}}) \in \underline{U}_{h,0}^k$ such that

$$a_h(\underline{u}_h, \underline{w}_h) = \ell_h(\underline{w}_h), \qquad \forall \underline{w}_h := (w_{\mathcal{T}}, w_{\mathcal{F}}) \in \underline{U}_{h,0}^k,$$

Degrees of freedom II

- Due to the hybridization the global number of DOF’s is bigger than a FEM approach.
- Compact stencil: due to face DOF’s involving only neighbors.
- Cell DOF’s are eliminated by static condensation, reducing the computational cost on the solver process.
- Cell DOF’s are recovered by local computations

Applying DISK to ALG

Local bilinear forms a_T and s_T on $\underline{\mathbf{U}}_T^k \times \underline{\mathbf{U}}_T^k$

- Diffusion term

$$a_T(\underline{\mathbf{v}}, \underline{\mathbf{w}}) := (\nabla_s \mathbf{r}_T^{k+1} \underline{\mathbf{v}}, \nabla_s \mathbf{r}_T^{k+1} \underline{\mathbf{w}})_T + s_T(\underline{\mathbf{v}}, \underline{\mathbf{w}}),$$

- Stabilization term: coupling cell and face unknowns

$$s_T(\underline{\mathbf{v}}, \underline{\mathbf{w}}) := \sum_{F \in \mathcal{F}_T} h_F^{-1} (\pi_F^k(\mathbf{v}_F - \hat{\mathbf{r}}_T^{k+1} \underline{\mathbf{v}}), \pi_F^k(\mathbf{w}_F - \hat{\mathbf{r}}_T^{k+1} \underline{\mathbf{w}}))_F$$

  Second velocity reconstruction $\hat{\mathbf{r}}_T^{k+1} : \underline{\mathbf{U}}_T^k \to \mathbb{P}_d^{k+1}(T)^d$

$$\hat{\mathbf{r}}_T^{k+1} = \mathbf{v}_T + (\mathbf{r}_T^{k+1} \underline{\mathbf{v}} - \pi_T^k \mathbf{r}_T^{k+1} \underline{\mathbf{v}})$$

- Stress-strain term

$$c_T(\boldsymbol{\tau}, \underline{\mathbf{v}}) = (\boldsymbol{\tau}, \nabla_s \mathbf{v}_T)_T + \sum_{F \in \mathcal{F}_T} (\boldsymbol{\tau} \cdot \mathbf{n}, \mathbf{v}_F - \mathbf{v}_T) \quad \text{on} \quad \mathfrak{L}^2(T) \times \underline{\mathbf{U}}_T^k.$$

- Global versions of the linear forms are obtained by cell-wise assembly.

DiSK-ALG

- Discrete weak formulation: Let $\boldsymbol{\sigma}^n$ and γ^n known, find $\underline{\mathbf{u}}_h \in \underline{\mathbf{U}}_{h,0}^k$ such that: $\forall \underline{\mathbf{v}}_h^{n+1} \in \underline{\mathbf{U}}_{h,0}^k$

$$2\alpha a_h(\underline{\mathbf{u}}_h^{n+1}, \underline{\mathbf{v}}_h^{n+1}) = \sum_{T\in\mathcal{T}_h} (\mathbf{f}, \mathbf{v}_T)_T - c_h(\boldsymbol{\sigma}^n - 2\alpha\gamma^n, \underline{\mathbf{v}}_h)$$

- Compute γ

$$\gamma^{n+1}(\mathbf{x}) = \begin{cases} 0 & \text{for} |\mathbf{X}^{n+1}(\mathbf{x})| \leqslant \sqrt{2}\tau_0 \\ \dfrac{1}{2(\alpha+\mu)} \left(|\mathbf{X}^{n+1}(\mathbf{x})| - \sqrt{2}\tau_0 \right) \dfrac{\mathbf{X}^{n+1}(\mathbf{x})}{|\mathbf{X}^{n+1}(\mathbf{x})|} & \text{for otherwise} \end{cases}$$

with $\mathbf{X}^{n+1}(\mathbf{x}) = \boldsymbol{\sigma}^n(\mathbf{x}) + 2\alpha\nabla_s\mathbf{r}_T^{k+1}\mathbf{u}^{n+1}(\mathbf{x})$.

- Update stress

$$\boldsymbol{\sigma}^{n+1} = \boldsymbol{\sigma}^n + 2\alpha(\nabla_s\mathbf{r}_T^{k+1}\mathbf{u}^{n+1} - \gamma^{n+1}).$$

Numerical results I

Test Setting

The cases are benchmarks consisting of an unidirectional source along the pipe-axis and no-slip conditions enforced on the walls.

- Test case 1: Poiseuille problem in 1D, analytical solution.
- Test case 2: Circular cross section problem, analytical solution.
- Test case 3: Square cross section problem, no analytical solution.

- The dimensionless Bingham number (Bi) is the ratio between the yield stress and the viscous stress.

Numerical Results I

- Fig. 8 showcases the agreement for tests 1 and 2 between the numerical and analytical solution.
- Computations are done using conforming meshes.

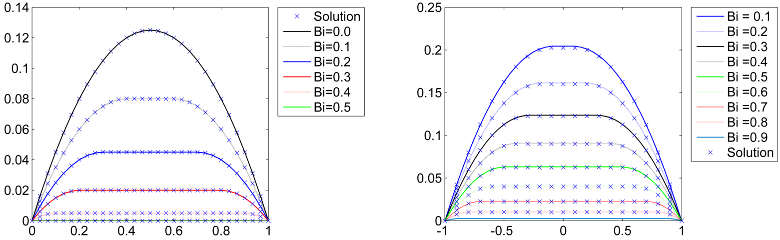

Figure: Velocity profiles for the 1D test case (left) and the circular pipe test case(right).

Numerical Results II

Mesh adapatation:

Features

- Non-conforming meshes.
- Control of the number of hanging nodes per face.
- Marker based on stress values at Gauss nodes

The challenge

- Capture of the transition boundaries: plug region in the center, a concentric annulus as shear zone and a dead region around the corners.

Levels of refinement

- Let $\mathcal{T}_h^0$ be the initial mesh and $\mathcal{T}_h^i$ the mesh after i- refinement steps.
- Let $T \in \mathcal{T}_i$ and denote its ancestor $T_0 \in \mathcal{T}_0$, such that $T_0 \subset T$.
- Labeling of levels: The level of T is the number of times T_0 has being partitioned to obtain T through the i-adaptive steps.
- After each marking process, check the difference of level be < 2, between neighbors.

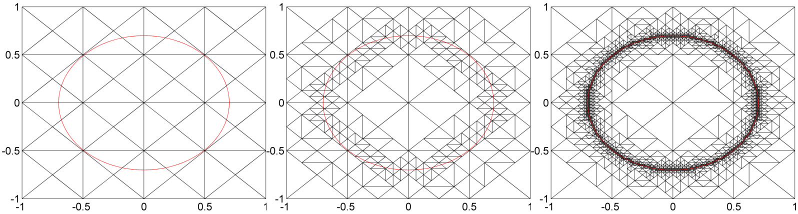

(a) Initial mesh, (b) 2nd adapted mesh, (c) 5th adapted mesh

Figure: Checking levels test

Numerical Results III

Circular pipe:
For fine meshes we obtained the expected behavior of the adaptation process, adapting around the inner red line (solid-liquid boundary).

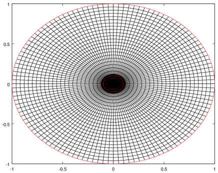

(a) Bi = 0.1

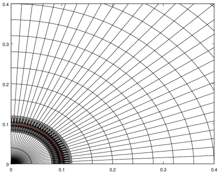

(b) zoom for Bi = 0.1

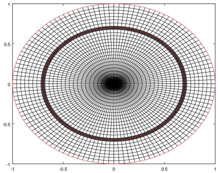

(c) Bi = 0.7

Figure: 1st step.

Numerical Results IV

Circular pipe: Coarse mesh

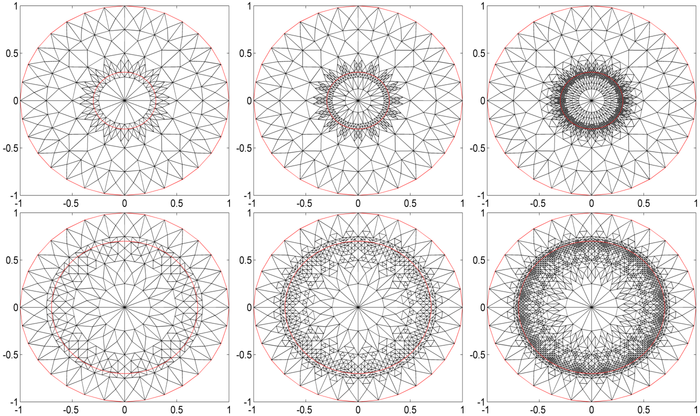

Figure: Mesh adaptation evolution for $Bi = 0.3$ (top) and $Bi = 0.3(\mathit{left})$.

Numerical Results: Square pipe

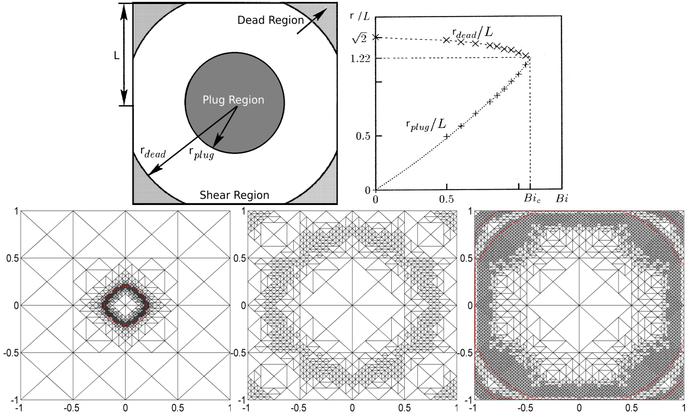

Figure: Mesh adaptation evolution for $Bi = 0.2$ (left),$Bi = 0.8(center)$ and $Bi = 1.0(right)$.

Future work

- Develop a Cut-Cell-DISK to simulate bubbles.
- hp-adaptivity: straightforward with DISK.
- Other viscoplastic models: Herschel-Bulkley.
- Use of cone programming optimization with DISK methods.

Thank you!

Thank you!

D. A. Di Pietro, A. Ern, and S. Lemaire.
An arbitrary-order and compact-stencil discretization of diffusion on general meshes based on local reconstruction operators.
Comput. Meth. Appl. Math., 14(4):461–472, 2014.
Open access (editor's choice).

M Fortin and Roland Glowinski.
Augmented lagrangian methods.
Elsevier, 1983.

Daniele A. Di Pietro and Alexandre Ern.
A hybrid high-order locking-free method for linear elasticity on general meshes.
Computer Methods in Applied Mechanics and Engineering, 283:1 – 21, 2015.